



Electric field induced topological phase transition and large enhancements of spin-orbit coupling and Curie temperature in two-dimensional ferromagnetic semiconductors

Jing-Yang You ¹, Xue-Juan Dong,² Bo Gu,^{1,3,*} and Gang Su ^{1,2,3,†}

¹*Kavli Institute for Theoretical Sciences and CAS Center for Excellence in Topological Quantum Computation, University of Chinese Academy of Sciences, Beijing 100190, China*

²*School of Physical Sciences, University of Chinese Academy of Sciences, Beijing 100049, China*

³*Physical Science Laboratory, Huairou National Comprehensive Science Center, Beijing 101400, China*



(Received 22 September 2020; revised 10 February 2021; accepted 16 February 2021; published 1 March 2021)

Tuning the topological and magnetic properties of materials by applying an electric field is widely used in spintronics. In this work, we find a topological phase transition from topologically trivial to nontrivial states at an external electric field of about 0.1 V/Å in a MnBi₂Te₄ monolayer that is a topologically trivial ferromagnetic semiconductor. It is shown that when electric field increases from 0 to 0.15 V/Å, the magnetic anisotropy energy (MAE) increases from about 0.1 to 6.3 meV, and the Curie temperature T_C increases from 13 to about 61 K. The increased MAE mainly comes from the enhanced spin-orbit coupling due to the applied electric field. The enhanced T_C can be understood from the enhanced p - d hybridization and decreased energy difference between p orbitals of Te atoms and d orbitals of Mn atoms. Moreover, we propose two Janus materials, MnBi₂Se₂Te₂ and MnBi₂S₂Te₂ monolayers with different internal electric polarizations, which can realize the quantum anomalous Hall effect (QAHE) with Chern numbers $C = 1$ and $C = 2$, respectively. Our study not only exposes the electric field induced exotic properties of the MnBi₂Te₄ monolayer but also proposes materials to realize QAHE in ferromagnetic Janus semiconductors with electric polarization.

DOI: [10.1103/PhysRevB.103.104403](https://doi.org/10.1103/PhysRevB.103.104403)

I. INTRODUCTION

The quantum anomalous Hall effect (QAHE) as a novel topological phase has attracted tremendous interest because of its potential applications in dissipationless spintronics [1–16]. The QAHE was first realized experimentally in a Cr-doped (Bi, Sb)₂Te₃ thin film at 30 mK [6] and later in a V-doped (Bi, Sb)₂Te₃ thin film at 25 mK [8] and a Cr-doped (Bi, Sb)₂Te₃ thin film at about 2 K [9]. Then, the QAHE was observed in a Cr- and V-codoped (Bi, Sb)₂Te₃ system at about 300 mK [13]. Since magnetic order that is stable at high temperature is essential for QAHE, we need to increase the ordering temperature of a magnetically doped topological insulator.

MnBi₂Te₄ as a platform to realize QAHE has received extensive study both in theory and in experiments [17,18]. MnBi₂Te₄ is composed of septuple Te-Bi-Te-Mn-Te-Bi-Te sequences and exhibits a van der Waals layered structure [19]. Bulk MnBi₂Te₄ is an antiferromagnetic insulator with a Néel temperature of 25 K [20,21], which presents the axion state [22]. Topological surface states with a diminished gap forming a characteristic Dirac cone attributed to multidomains of different magnetization orientations were observed in the antiferromagnetic topological insulator MnBi₂Te₄ [23]. The heterostructures (Bi₂Te₃)_{*n*}(MnBi₂Te₄) were extensively studied to realize QAHE [24–30]. The MnBi₂Te₄ monolayer is a topologically trivial ferromagnetic semiconductor [31–33],

while its multilayers host states alternating between QAH and zero-plateau QAH for odd and even number of monolayers, respectively [33]. In a five-septuple-layer MnBi₂Te₄, the QAHE was observed at 1.4 K, and the quantization temperature can be increased up to 6.5 K by an external magnetic field to align all layers ferromagnetically [34]. A high-Chern-number QHE without Landau levels was obtained in 10-septuple-layer MnBi₂Te₄ under applied magnetic field and back gate voltages [35]. In six-septuple-layer MnBi₂Te₄, the axion insulator state occurs over a wide magnetic field range and at relatively high temperatures, while a moderate magnetic field can drive the axion insulator phase to a Chern insulator phase with QAHE [36].

Tuning the energy gap is widely used in spintronics because it can optimize the properties of materials and make materials have better performance in devices. There are several ways to tune the energy bands, such as by an electric field [37–40], strain [41–43], doping [44–47], vacancy [48–50], surface modification [44,51], and so on. Tuning energy bands by an external electric field has some advantages: the magnitude and direction of the external electric field can be arbitrarily controlled; applying the external electric field is feasible and easy to realize in experiments. Graphene is a two-dimensional (2D) material with zero band gap, which restricts its application in electronic devices. After applying a gate voltage, the inversion symmetry is broken, and a nonzero band gap is opened [52–56]. The band engineering by external electric fields was also performed in MoS₂ [57].

In this work, we study properties of the MnBi₂Te₄ monolayer controlled by an electric field. With the increase of

*gubo@ucas.ac.cn

†gsu@ucas.ac.cn

electric field, the band gap decreases, the band inversion with a topological phase transition occurs at an electric field of about 0.1 V/\AA , and the system then enters into a topological state. With the electric field ranging from 0 to 0.15 V/\AA , the magnetic anisotropy energy (MAE) increases from about 0.1 to 6.3 meV , and the Curie temperature T_C increases from 13 to about 61 K . The increased MAE mainly comes from the enhanced spin-orbit coupling (SOC) due to the applied electric field. By means of the superexchange picture, the enhanced T_C can be understood from the enhanced p - d hybridization and decreased energy difference between p orbitals of Te atoms and d orbitals of Mn atoms. Inspired by the electric field induced topological phase transition, we propose the 2D Janus materials $\text{MnBi}_2\text{Se}_2\text{Te}_2$ and $\text{MnBi}_2\text{S}_2\text{Te}_2$ with different internal electric polarizations, which can realize QAHE. Our findings not only reveal the electric field induced exotic properties of the MnBi_2Te_4 monolayer but also present an idea to realize QAHE in ferromagnetic Janus materials with electric polarizations.

II. CALCULATION METHOD

Our first-principles calculations were based on density functional theory (DFT) as implemented in the Vienna Ab initio Simulation Package (VASP) [58], using the projector augmented-wave method [59]. The generalized gradient approximation (GGA) with the Perdew-Burke-Ernzerhof [60] realization was adopted for the exchange-correlation functional. We set the on-site effective Hubbard interaction $U = 4 \text{ eV}$ in considering the electron correlation of $3d$ electrons of Mn atoms. The monolayer was placed under a vacuum layer of 15 \AA . The plane-wave cutoff energy was set to 550 eV . A Monkhorst-Pack k -point mesh [61] with a size of $19 \times 19 \times 1$ was used for the Brillouin zone sampling. The crystal structure was optimized until the forces on the ions were less than 0.0001 eV/\AA , and the total energy was converged to 10^{-8} eV with the Gaussian smearing method. The interaction of the magnetic dipoles was taken into account in calculations of the magnetic anisotropy energies. The phonon spectra were obtained in a $4 \times 4 \times 1$ supercell with the PHONOPY package [62]. The surface spectrum was calculated using the Wannier functions and the iterative Green's function method [63–66].

III. MONOLAYER MnBi_2Te_4

Monolayer MnBi_2Te_4 can be grown in a quintuple layer of Bi_2Te_3 and a bilayer of MnTe with the molecular beam epitaxy method [67]. The crystal structure of monolayer MnBi_2Te_4 is shown in Fig. 1. The space group is $P\bar{3}m1$ (No. 164) with an optimized lattice constant $a = 4.34 \text{ \AA}$. Monolayer MnBi_2Te_4 is a ferromagnetic semiconductor with out-of-plane magnetization, and the Curie temperature T_C of its septuple-layer film is about 20 K [67]. Our estimated Curie temperature of monolayer MnBi_2Te_4 is comparable to that of its film [67,68]. The atom-projected band structure of monolayer MnBi_2Te_4 without electric field is plotted in Fig. 2(a), from which one can observe that the bottom of the conduction band of monolayer MnBi_2Te_4 is mainly attributed to Bi-1 and Bi-2 atoms, while the main contribution to the top of the valence bands is from Te-4 and Te-1 atoms. Because

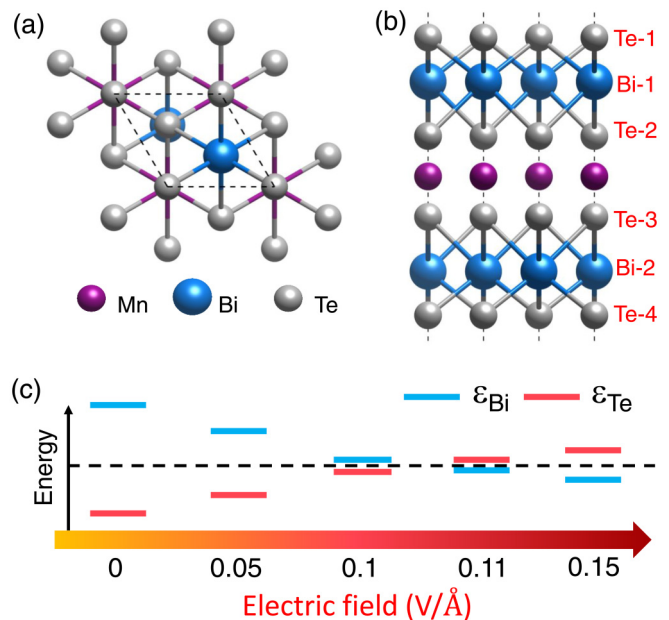


FIG. 1. Crystal structure of monolayer MnBi_2Te_4 . The (a) top and (b) side views of monolayer MnBi_2Te_4 , where the atoms are labeled with elements and the atomic layer number in (b). (c) The evolution of the top of the valence band and the bottom of the conduction band relative to their energy center at the Γ point with increasing electric field.

of the inversion symmetry, Bi-1 and Bi-2 atoms give equal contributions to the density of states of the bottom of the conduction bands at the Γ point, and Te-1 and Te-4 atoms contribute equally to the density of states of the top of the valence bands at the Γ point.

IV. MONOLAYER MnBi_2Te_4 UNDER AN ELECTRIC FIELD

By applying an electric field E normal to the atoms' plane, we can tune the properties of monolayer MnBi_2Te_4 . The effect of electric field on the properties of monolayer MnBi_2Te_4 is summarized in Table S1 in the Supplemental Material [68]. There are three main changes in the properties of monolayer MnBi_2Te_4 with increasing electric field, including the changes in the band gap, magnetic anisotropy, and exchange integral.

A. Evolution of the band gap under an electric field

The band structure of monolayer MnBi_2Te_4 varies with increasing electric field without a big deformation of profiles but with a remarkable change in the band gap, as shown in Fig. 2. The evolution of the band gap at the Γ point with the electric field is schematically plotted in Fig. 1(c). The direct band gap at the Γ point [Fig. 2(e)] and the global band gap increase with increasing electric field lower than 0.1 V/\AA . This is intuitive because, on the one hand, the electric field E breaks the inversion symmetry of monolayer MnBi_2Te_4 , resulting in degeneracy-broken Bi-1 and Bi-2 and Te-1 and Te-4 atoms at the Γ point and, on the other hand, the effect of electric field on the upper triple Te-Bi-Te layers consisting of Te-1, Bi-1, and Te-2 atoms is equivalent to electron doping, while for the lower triple Te-Bi-Te layers consisting of Te-3, Bi-2, and

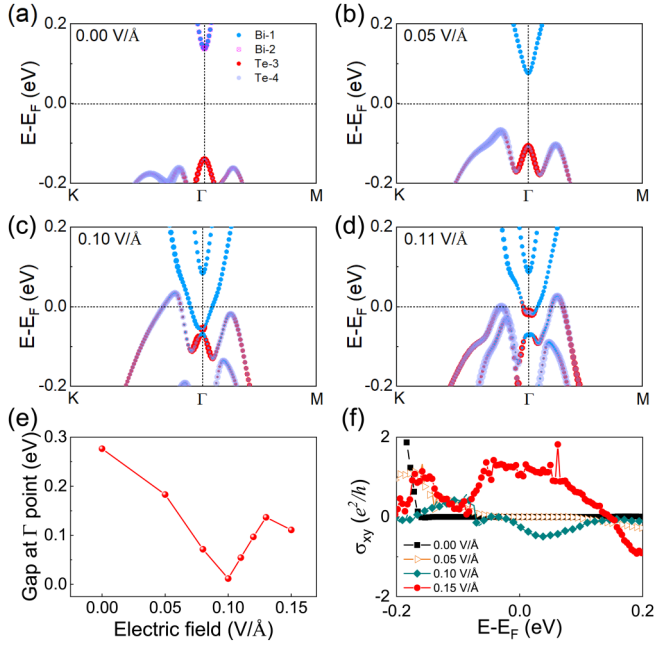


FIG. 2. Electric field induced topological phase transition. Atom-projected electronic band structures of monolayer MnBi_2Te_4 under an electric field of (a) 0.00, (b) 0.05, (c) 0.10, and (d) 0.11 $\text{V}/\text{\AA}$. The electric field dependent (e) direct band gap at the Γ point and (f) anomalous Hall conductivity. The results were obtained by the GGA+SOC+ U calculations with $U = 4 \text{ eV}$.

Te-4 atoms it corresponds to hole doping. Thus, for the cation Bi-1, its energy level moves downward close to Fermi level, while for anion Te-4, its energy level moves upward close to Fermi level. This analysis is also verified by our DFT results, as shown in Fig. 2. Therefore, the energy levels of Bi-1 and Te-4 atoms should be touched at a proper electric field, which is about 0.1 $\text{V}/\text{\AA}$ in our calculations. When the electric field continues to increase to 0.11 $\text{V}/\text{\AA}$, an inversion of the energy bands occurs at the Γ point [Fig. 2(d)] with a topological phase transition from a topological trivial state to a nontrivial state with nonzero Chern number $C = 1$. However, because there is no global energy gap, we cannot observe quantized anomalous Hall conductivity (AHC), but it can adiabatically evolve to the quantum anomalous Hall insulating state. When the electric field continues to increase from 0.13 to 0.15 $\text{V}/\text{\AA}$, the direct band gap at the Γ point decreases, and the system turns into the topological state with $C = 2$. Although there is also no global gap, it is interesting to note that a relatively flat plateau of AHC occurs with $E = 0.15 \text{ V}/\text{\AA}$ near the Fermi level, as shown in Fig. 2(f).

B. Magnetic anisotropy of the MnBi_2Te_4 monolayer under an electric field

Besides the topological phase transition, the electric field also dramatically influences MAE, where MAE means the energy difference per MnBi_2Te_4 formula unit between the out-of-plane and in-plane ferromagnetic configurations. The electric field E dependent MAE is plotted in Fig. 3(a). From Fig. 3(a), one may observe that MAE increases with increasing E . MAEs are usually related to the SOC; thus, the increase

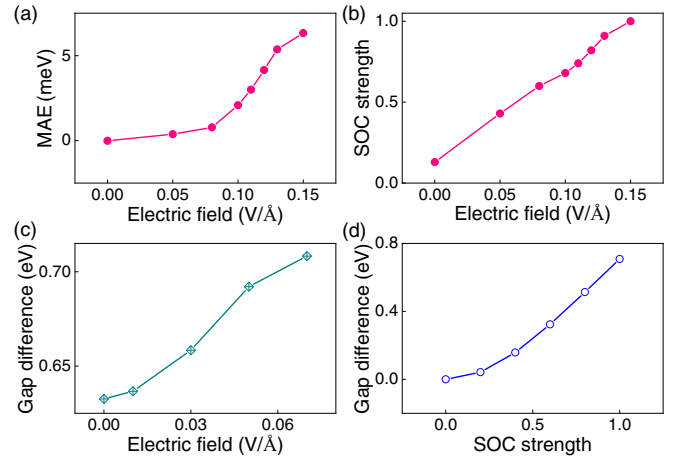


FIG. 3. Electric field enhanced spin-orbit coupling. The (a) electric field and (b) SOC strength dependent MAE, where MAE means the energy difference per MnBi_2Te_4 formula unit between the in-plane and out-of-plane magnetic configurations and the SOC strength under an electric field of 0.15 $\text{V}/\text{\AA}$ is set to 1. The (c) electric field and (d) SOC strength dependent gap difference between the gaps without and with SOC.

of MAE may come from the enhanced SOC because of the electric field. To verify this observation, we extracted the dependence of MAE on the SOC strength with an electric field of 0.15 $\text{V}/\text{\AA}$ from DFT calculations and obtained the electric field dependent SOC strength by comparing the MAE under different electric fields and SOC strength as plotted in Fig. 3(b). It is obvious that the SOC is enhanced with increasing electric field. A larger AHC σ_{xy} is expected in monolayer MnBi_2Te_4 with enhanced SOC. We calculated the AHC with electric fields of 0.05, 0.10, and 0.15 $\text{V}/\text{\AA}$, as shown in Fig. 2(f). Enhanced SOC can also be seen from the enhanced AHC, as shown in Fig. 2(f), and the gap difference between the band gaps without SOC and with SOC, as shown in Figs. 3(c) and 3(d), with increasing electric field. The Mn local magnetic moment is not sensitive to the electric field, and in the range of electric field we studied, it remains at about $4.5\mu_B$.

C. Curie temperature under an electric field

The exchange integral J has a similar dependence on the electric field; that is, the exchange integral increases with an increase of E , as shown in Fig. 4(a). The increase in the exchange integral J can be interpreted by the superexchange interaction [69–71], where the ferromagnetic (FM) coupling is expected since the Mn-Te-Mn bond angle is close to 90° . The indirect FM coupling between Mn atoms is proportional to the direct antiferromagnetic (AFM) coupling between neighboring Mn and Te atoms. The magnitude of this direct AFM coupling can be roughly estimated as $J_{pd} = |V_{pd}|^2/|E_p - E_d|$, where $|V_{pd}|$ is the hopping matrix element between p orbitals of Te and d orbitals of Mn and $|E_p - E_d|$ is the energy difference between them. By using maximally localized Wannier orbital projections, the dominant hopping matrix elements $|V_{pd}|$ and their corresponding energy differences $|E_p - E_d|$ can be obtained for monolayer MnBi_2Te_4 without E and

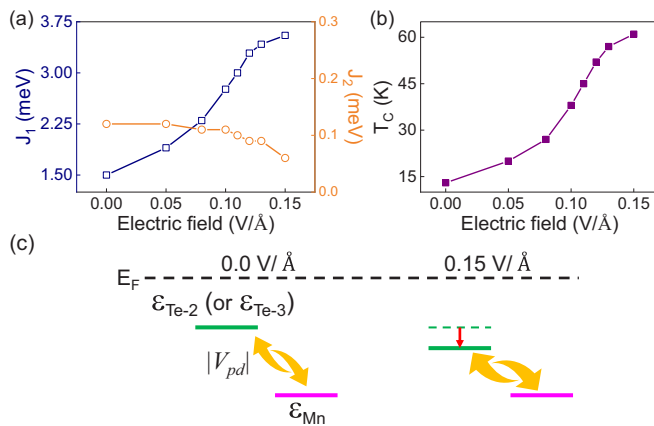


FIG. 4. Electric field enhanced Curie temperature. The evolution of the (a) exchange integrals and (b) Curie temperature with electric field. (c) The schematic diagram of the micromechanism of enhanced Curie temperature under electric field.

with $E = 0.15 \text{ V/\AA}$, respectively, as listed in Table S2. The enhanced direct AFM coupling with increasing electric field comes from the enhanced $p-d$ hybridization owing to the increase in hopping and the decrease in the energy difference between p orbitals of Te and d orbitals of Mn. It can be understood from the fact that the energy levels of Mn atoms are relatively deep in MnBi_2Te_4 , and the electric field drives the energy levels of the upper and lower Te layers near the Mn layer to move downward, resulting in the decrease of the energy level difference and the enhancement of the overlaps between p orbitals of Te and d orbitals of Mn atoms, as schematically depicted in Fig. 4(c).

The calculated Curie temperature based on the isotropic Heisenberg model with single-ion anisotropy using Monte Carlo simulation is listed in Table S1. It can be seen that for MnBi_2Te_4 with $E = 0.15 \text{ V/\AA}$ the Curie temperature is even about 4.5 times larger than that without E , as shown in Fig. 4(b).

V. MONOLAYER $\text{MnBi}_2\text{Se}_2\text{Te}_2$ AND $\text{MnBi}_2\text{S}_2\text{Te}_2$ FOR THE QAHE

Inspired by the above study, in which an electric field can tune the energy band and induce a topological phase transition in the MnBi_2Te_4 monolayer, we propose a 2D Janus structure, the $\text{MnBi}_2\text{Se}_2\text{Te}_2$ monolayer, based on the MnBi_2Te_4 monolayer. Janus crystals represent a class of 2D materials with different atomic species on their upper and lower facets. The Janus $\text{MnBi}_2\text{Se}_2\text{Te}_2$ monolayer can be obtained by substituting the upper triple Te-Bi-Te layers of the MnBi_2Te_4 monolayer with triple Se-Bi-Se layers. The stability of the $\text{MnBi}_2\text{Se}_2\text{Te}_2$ monolayer was checked by its phonon spectra, molecular dynamic simulation, and formation energy [68]. Because of the different electronegativities of Se and Te, the $\text{MnBi}_2\text{Se}_2\text{Te}_2$ monolayer possesses spontaneous electric polarization of about 0.44 e\AA . The $\text{MnBi}_2\text{Se}_2\text{Te}_2$ monolayer exhibits a ferromagnetic ground state with the in-plane magnetization, and its Curie temperature is estimated to be 14.3 K . Due to the small magnetic anisotropy, the magnetization direction can be tuned from in plane to out of plane by a

small magnetic field or strain. The band structure of the $\text{MnBi}_2\text{Se}_2\text{Te}_2$ monolayer shows a full band gap of about 44 meV , as shown in Fig. 5(a). The calculation of anomalous Hall conductivity shows a plateau at the Fermi level, which corresponds to a Chern number $C = 1$, indicating the QAHE state, as shown in Fig. 5(b). As discussed above for the MnBi_2Te_4 monolayer, when the system turns into the topological phase, the energy gap increases first and then decreases, and the Curie temperature keeps increasing with the increase of the electric field. This is verified again in the $\text{MnBi}_2\text{Se}_2\text{Te}_2$ monolayer, where the electric field enhances the Curie temperature and changes the band gap as shown in Fig. 5(c).

For the Janus $\text{MnBi}_2\text{S}_2\text{Te}_2$ monolayer, its spontaneous electric polarization is about 0.73 e\AA , which is larger than that for the $\text{MnBi}_2\text{Se}_2\text{Te}_2$ monolayer; thus, a larger band gap and higher Curie temperature are expected in the $\text{MnBi}_2\text{S}_2\text{Te}_2$ monolayer according to the above discussion. The $\text{MnBi}_2\text{S}_2\text{Te}_2$ monolayer holds a ferromagnetic ground state with out-of-plane magnetization, and its Curie temperature is estimated to be 30 K . The $\text{MnBi}_2\text{S}_2\text{Te}_2$ monolayer has a global band gap of about 80 meV , as shown in Fig. 5(d). The topologically nontrivial band structure of the $\text{MnBi}_2\text{S}_2\text{Te}_2$ monolayer is characterized by a nonzero Chern number $C = 2$ with a quantized charge Hall plateau of $2e^2/h$ and two gapless chiral edge states connecting the valence and conduction bands, as shown in Figs. 5(e) and 5(f).

To check the influence of the Hubbard U on the QAHE, we calculate the anomalous Hall conductivity with $U = 3, 4$, and 5 for the $\text{MnBi}_2\text{Se}_2\text{Te}_2$ and $\text{MnBi}_2\text{S}_2\text{Te}_2$ monolayers, as shown in Fig. S4. The results show that by varying the Hubbard U from 3 to 5 eV , the QAHE states in both $\text{MnBi}_2\text{Se}_2\text{Te}_2$ and $\text{MnBi}_2\text{S}_2\text{Te}_2$ remain, but the band gap is slightly changed.

In monolayers one would expect a gap to open at an energy scale set by the overlap of the edge mode wave functions on the top and bottom surfaces. The gaps opened by the mixture of the top and bottom surfaces for Janus $\text{MnBi}_2\text{Se}_2\text{Te}_2$ and $\text{MnBi}_2\text{S}_2\text{Te}_2$ are 118 and 121 meV , respectively, and the corresponding magnetic exchange energies of the above Janus materials are 140 and 161 meV . In both cases, the gaps are smaller than the magnetic exchange energy, supporting the QAHE states.

According to the calculated results of the phonon spectra, molecular dynamics simulation, and the formation energy for Janus $\text{MnBi}_2\text{Se}_2\text{Te}_2$ and $\text{MnBi}_2\text{S}_2\text{Te}_2$, we found that they are both energetically and dynamically stable and are feasible in experiments because of their exothermic reactions and much lower formation energy than that of MnBi_2Te_4 [68]. Thus, one may expect to grow the bulk materials first and then exfoliate them. Alternatively, Janus $\text{MnBi}_2\text{Se}_2\text{Te}_2$ can be grown in quintuple layers of Bi_2Te_3 and Bi_2Se_3 and a bilayer of MnTe with the molecular beam epitaxy method.

VI. SUMMARY

In this work, we systematically investigated the properties of monolayer MnBi_2Te_4 under electric field. It was found that the electric field can induce a topological phase transition

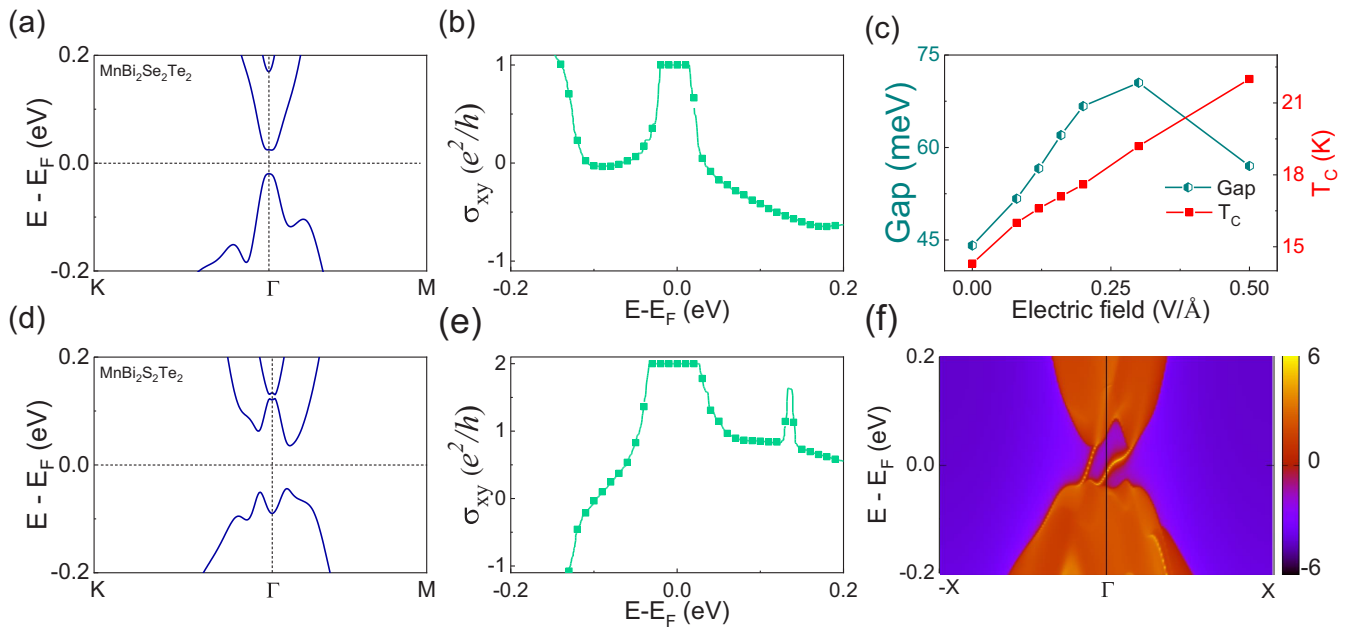


FIG. 5. QAHE in monolayer $\text{MnBi}_2\text{Se}_2\text{Te}_2$ and $\text{MnBi}_2\text{S}_2\text{Te}_2$. (a) Band structure, (b) AHC, and (c) electric field dependent band gap and Curie temperature of monolayer $\text{MnBi}_2\text{Se}_2\text{Te}_2$. (d) Band structure, (e) AHC, and (f) edge states of monolayer $\text{MnBi}_2\text{S}_2\text{Te}_2$.

from a topologically trivial state to a nontrivial state. It was also observed that the MAE and T_C of MnBi_2Te_4 monolayer are dramatically enhanced with the increase of electric field. The increased MAE mainly comes from the enhanced SOC due to the electric field. In terms of the superexchange picture, the enhanced T_C can be understood from the enhanced p - d hybridization and decreased energy difference between p orbitals of Te atoms and d orbitals of Mn atoms. In addition, we proposed the Janus monolayers $\text{MnBi}_2\text{Se}_2\text{Te}_2$ and $\text{MnBi}_2\text{S}_2\text{Te}_2$ with different spontaneous electric polarizations, which can realize the QAHE with Chern numbers $C = 1$ and $C = 2$, respectively. Our results will spur more studies on properties of the MnBi_2Te_4 monolayer under an electric field and also provide candidates to realize the QAHE in ferromagnetic semiconductors with electric polarization that would be particularly interesting in electrically controlled spintronic devices.

ACKNOWLEDGMENTS

This work is supported in part by the National Key R&D Program of China (Grant No. 2018YFA0305800), the Strategic Priority Research Program of the Chinese Academy of Sciences (Grant No. XDB28000000), the National Natural Science Foundation of China (Grant No. 11834014), and the Beijing Municipal Science and Technology Commission (Grant No. Z191100007219013). B.G. is also supported by the National Natural Science Foundation of China (Grants No. Y81Z01A1A9 and No. 12074378), the Chinese Academy of Sciences (Grants No. Y929013EA2 and No. E0EG4301X2), the University of the Chinese Academy of Sciences (Grant No. 110200M208), the Strategic Priority Research Program of the Chinese Academy of Sciences (Grant No. XDB33000000), and the Beijing Natural Science Foundation (Grant No. Z190011).

J.-Y.Y. and X.-J.D. contributed equally to this work.

- [1] F. D. M. Haldane, *Phys. Rev. Lett.* **61**, 2015 (1988).
- [2] M. Onoda and N. Nagaosa, *Phys. Rev. Lett.* **90**, 206601 (2003).
- [3] C.-X. Liu, X.-L. Qi, X. Dai, Z. Fang, and S.-C. Zhang, *Phys. Rev. Lett.* **101**, 146802 (2008).
- [4] C. Wu, *Phys. Rev. Lett.* **101**, 186807 (2008).
- [5] R. Yu, W. Zhang, H.-J. Zhang, S.-C. Zhang, X. Dai, and Z. Fang, *Science* **329**, 61 (2010).
- [6] C.-Z. Chang, J. Zhang, X. Feng, J. Shen, Z. Zhang, M. Guo, K. Li, Y. Ou, P. Wei, L.-L. Wang, Z.-Q. Ji, Y. Feng, S. Ji, X. Chen, J. Jia, X. Dai, Z. Fang, S.-C. Zhang, K. He, Y. Wang, L. Lu, X.-C. Ma, and Q.-K. Xue, *Science* **340**, 167 (2013).
- [7] J. Wu, J. Liu, and X.-J. Liu, *Phys. Rev. Lett.* **113**, 136403 (2014).
- [8] C.-Z. Chang, W. Zhao, D. Y. Kim, H. Zhang, B. A. Assaf, D. Heiman, S.-C. Zhang, C. Liu, M. H. W. Chan, and J. S. Moodera, *Nat. Mater.* **14**, 473 (2015).
- [9] M. Mogi, R. Yoshimi, A. Tsukazaki, K. Yasuda, Y. Kozuka, K. S. Takahashi, M. Kawasaki, and Y. Tokura, *Appl. Phys. Lett.* **107**, 182401 (2015).
- [10] C.-X. Liu, S.-C. Zhang, and X.-L. Qi, *Annu. Rev. Condens. Matter Phys.* **7**, 301 (2016).
- [11] L. Si, O. Janson, G. Li, Z. Zhong, Z. Liao, G. Koster, and K. Held, *Phys. Rev. Lett.* **119**, 026402 (2017).

- [12] J.-Y. You, C. Chen, Z. Zhang, X.-L. Sheng, S. A. Yang, and G. Su, *Phys. Rev. B* **100**, 064408 (2019).
- [13] Y. Ou, C. Liu, G. Jiang, Y. Feng, D. Zhao, W. Wu, X.-X. Wang, W. Li, C. Song, L.-L. Wang, W. Wang, W. Wu, Y. Wang, K. He, X.-C. Ma, and Q.-K. Xue, *Adv. Mater.* **30**, 1703062 (2017).
- [14] K. He, Y. Wang, and Q.-K. Xue, *Annu. Rev. Condens. Matter Phys.* **9**, 329 (2018).
- [15] J.-Y. You, Z. Zhang, B. Gu, and G. Su, *Phys. Rev. Appl.* **12**, 024063 (2019).
- [16] Y. Li, J. Li, Y. Li, M. Ye, F. Zheng, Z. Zhang, J. Fu, W. Duan, and Y. Xu, *Phys. Rev. Lett.* **125**, 086401 (2020).
- [17] M. M. Otrokov, T. V. Menshchikova, M. G. Vergniory, I. P. Rusinov, A. Y. Vyazovskaya, Y. M. Koroteev, G. Bihlmayer, A. Ernst, P. M. Echenique, A. Arnau, and E. V. Chulkov, *2D Mater.* **4**, 025082 (2017).
- [18] M. M. Otrokov *et al.*, *Nature (London)* **576**, 416 (2019).
- [19] D. S. Lee, T.-H. Kim, C.-H. Park, C.-Y. Chung, Y. S. Lim, W.-S. Seo, and H.-H. Park, *CrystEngComm* **15**, 5532 (2013).
- [20] J. Cui, M. Shi, H. Wang, F. Yu, T. Wu, X. Luo, J. Ying, and X. Chen, *Phys. Rev. B* **99**, 155125 (2019).
- [21] H. Li, S. Liu, C. Liu, J. Zhang, Y. Xu, R. Yu, Y. Wu, Y. Zhang, and S. Fan, *Phys. Chem. Chem. Phys.* **22**, 556 (2020).
- [22] D. Zhang, M. Shi, T. Zhu, D. Xing, H. Zhang, and J. Wang, *Phys. Rev. Lett.* **122**, 206401 (2019).
- [23] Y. J. Chen, L. X. Xu, J. H. Li, Y. W. Li, H. Y. Wang, C. F. Zhang, H. Li, Y. Wu, A. J. Liang, C. Chen, S. W. Jung, C. Cacho, Y. H. Mao, S. Liu, M. X. Wang, Y. F. Guo, Y. Xu, Z. K. Liu, L. X. Yang, and Y. L. Chen, *Phys. Rev. X* **9**, 041040 (2019).
- [24] R. C. Vidal, A. Zeugner, J. I. Facio, R. Ray, M. H. Haghghi, A. U.B Wolter, L. T. CorredorBohorquez, F. Cagliaris, S. Moser, T. Figgemeier, T. R.F. Peixoto, H. B. Vasili, M. Valvidares, S. Jung, C. Cacho, A. Alfonsov, K. Mehlawat, V. Kataev, C. Hess, M. Richter, B. Buchner, J. van den Brink, M. Ruck, F. Reinert, H. Bentmann, and A. Isaeva, *Phys. Rev. X* **9**, 041065 (2019).
- [25] Z. S. Aliev, I. R. Amiraslanov, D. I. Nasonova, A. V. Shevelkov, N. A. Abdullayev, Z. A. Jahangirli, E. N. Orujlu, M. M. Otrokov, N. T. Mamedov, M. B. Babanly, and E. V. Chulkov, *J. Alloys Compd.* **789**, 443 (2019).
- [26] H. Deng, Z. Chen, A. Wołos, M. Konczykowski, K. Sobczak, J. Sitnicka, I. V. Fedorchenko, J. Borysiuk, T. Heider, Ł. Pluciński, K. Park, A. B. Georgescu, J. Cano, and L. Krusin-Elbaum, *Nat. Phys.* **17**, 36 (2021).
- [27] C. Lei, S. Chen, and A. H. MacDonald, *Proc. Natl. Acad. Sci. U.S.A.* **117**, 27224 (2020).
- [28] E. D. L. Rienks *et al.*, *Nature (London)* **576**, 423 (2019).
- [29] C. Hu *et al.*, *Sci. Adv.* **6**, eaba4275 (2020).
- [30] I. I. Klimovskikh *et al.*, *npj Quantum Mater.* **5**, 54 (2020).
- [31] J. Li, Y. Li, S. Du, Z. Wang, B.-L. Gu, S.-C. Zhang, K. He, W. Duan, and Y. Xu, *Sci. Adv.* **5**, eaaw5685 (2019).
- [32] Y. Li, Z. Jiang, J. Li, S. Xu, and W. Duan, *Phys. Rev. B* **100**, 134438 (2019).
- [33] M. M. Otrokov, I. P. Rusinov, M. Blanco-Rey, M. Hoffmann, A. Y. Vyazovskaya, S. V. Eremeev, A. Ernst, P. M. Echenique, A. Arnau, and E. V. Chulkov, *Phys. Rev. Lett.* **122**, 107202 (2019).
- [34] Y. Deng, Y. Yu, M. Z. Shi, Z. Guo, Z. Xu, J. Wang, X. H. Chen, and Y. Zhang, *Science* **367**, 895 (2020).
- [35] J. Ge, Y. Liu, J. Li, H. Li, T. Luo, Y. Wu, Y. Xu, and J. Wang, *Natl. Sci. Rev.* **7**, 1280 (2020).
- [36] C. Liu, Y. Wang, H. Li, Y. Wu, Y. Li, J. Li, K. He, Y. Xu, J. Zhang, and Y. Wang, *Nat. Mater.* **19**, 522 (2020).
- [37] M. Weisheit, S. Fahler, A. Marty, Y. Souche, C. Poinignon, and D. Givord, *Science* **315**, 349 (2007).
- [38] Y. Deng, Y. Yu, Y. Song, J. Zhang, N. Z. Wang, Z. Sun, Y. Yi, Y. Z. Wu, S. Wu, J. Zhu, J. Wang, X. H. Chen, and Y. Zhang, *Nature (London)* **563**, 94 (2018).
- [39] S. Jiang, L. Li, Z. Wang, K. F. Mak, and J. Shan, *Nat. Nanotechnol.* **13**, 549 (2018).
- [40] S. Du, P. Tang, J. Li, Z. Lin, Y. Xu, W. Duan, and A. Rubio, *Phys. Rev. Research* **2**, 022025(R) (2020).
- [41] Z. H. Ni, T. Yu, Y. H. Lu, Y. Y. Wang, Y. P. Feng, and Z. X. Shen, *ACS Nano* **3**, 483 (2009).
- [42] X. C. Liu, H. W. Zhang, and K. Lu, *Science* **342**, 337 (2013).
- [43] X.-J. Dong, J.-Y. You, B. Gu, and G. Su, *Phys. Rev. Appl.* **12**, 014020 (2019).
- [44] D. M. Sim, M. Kim, S. Yim, M.-J. Choi, J. Choi, S. Yoo, and Y. S. Jung, *ACS Nano* **9**, 12115 (2015).
- [45] J.-Y. You, B. Gu, and G. Su, *Sci. Rep.* **9**, 20116 (2019).
- [46] T. Ahmed, N. A. Modine, and J.-X. Zhu, *Appl. Phys. Lett.* **107**, 043903 (2015).
- [47] J.-Y. You, B. Gu, and G. Su, *Phys. Rev. B* **101**, 184521 (2020).
- [48] Z. Chen, B. Ge, W. Li, S. Lin, J. Shen, Y. Chang, R. Hanus, G. J. Snyder, and Y. Pei, *Nat. Commun.* **8**, 13828 (2017).
- [49] Y. Liu, C. Ma, Q. Zhang, W. Wang, P. Pan, L. Gu, D. Xu, J. Bao, and Z. Dai, *Adv. Mater.* **31**, 1900062 (2019).
- [50] F. Hou, Q. Yao, C.-S. Zhou, X.-M. Ma, M. Han, Y.-J. Hao, X. Wu, Y. Zhang, H. Sun, C. Liu, Y. Zhao, Q. Liu, and J. Lin, *ACS Nano* **14**, 11262 (2020).
- [51] S. K. Nemani, R. K. Annavarapu, B. Mohammadian, A. Raiyan, J. Heil, M. A. Haque, A. Abdelaal, and H. Sojoudi, *Adv. Mater. Interfaces* **5**, 1801247 (2018).
- [52] T. Ohta, A. Bostwick, T. Seyller, K. Horn, and E. Rotenberg, *Science* **313**, 951 (2006).
- [53] H. Min, B. Sahu, S. K. Banerjee, and A. H. MacDonald, *Phys. Rev. B* **75**, 155115 (2007).
- [54] Y. Zhang, T.-T. Tang, C. Girit, Z. Hao, M. C. Martin, A. Zettl, M. F. Crommie, Y. R. Shen, and F. Wang, *Nature (London)* **459**, 820 (2009).
- [55] K. F. Mak, C. H. Lui, J. Shan, and T. F. Heinz, *Phys. Rev. Lett.* **102**, 256405 (2009).
- [56] C. H. Lui, Z. Li, K. F. Mak, E. Cappelluti, and T. F. Heinz, *Nat. Phys.* **7**, 944 (2011).
- [57] C.-P. Lu, G. Li, J. Mao, L.-M. Wang, and E. Y. Andrei, *Nano Lett.* **14**, 4628 (2014).
- [58] G. Kresse and J. Furthmüller, *Phys. Rev. B* **54**, 11169 (1996).
- [59] P. E. Blöchl, *Phys. Rev. B* **50**, 17953 (1994).
- [60] J. P. Perdew, K. Burke, and M. Ernzerhof, *Phys. Rev. Lett.* **77**, 3865 (1996).
- [61] H. J. Monkhorst and J. D. Pack, *Phys. Rev. B* **13**, 5188 (1976).
- [62] A. Togo and I. Tanaka, *Scr. Mater.* **108**, 1 (2015).
- [63] N. Marzari and D. Vanderbilt, *Phys. Rev. B* **56**, 12847 (1997).
- [64] I. Souza, N. Marzari, and D. Vanderbilt, *Phys. Rev. B* **65**, 035109 (2001).
- [65] Q. Wu, S. Zhang, H.-F. Song, M. Troyer, and A. A. Soluyanov, *Comput. Phys. Commun.* **224**, 405 (2018).

- [66] M. P. L. Sancho, J. M. L. Sancho, J. M. L. Sancho, and J. Rubio, *J. Phys. F* **15**, 851 (1985).
- [67] Y. Gong *et al.*, *Chin. Phys. Lett.* **36**, 076801 (2019).
- [68] See Supplemental Material at <http://link.aps.org/supplemental/10.1103/PhysRevB.103.104403> for DFT results on estimated Curie temperature and stability of MnBi_2Te_4 , $\text{MnBi}_2\text{Se}_2\text{Te}_2$, and $\text{MnBi}_2\text{S}_2\text{Te}_2$.
- [69] J. B. Goodenough, *Phys. Rev.* **100**, 564 (1955).
- [70] P. W. Anderson, *Phys. Rev.* **115**, 2 (1959).
- [71] J. Kanamori, *J. Appl. Phys.* **31**, S14 (1960).